Characterization and Visualization of Vesicles in the Endo-Lysosomal Pathway with Surface-Enhanced Raman Spectroscopy and Chemometrics

Anna Huefner[♪†‡], *Wei-Li Kuan*[†], *Karin H. Müller*[§], *Jeremy N. Skepper*[§], *Roger A. Barker*[†], *Sumeet Mahajan*[‡]*

[♪]Sector for Biological and Soft Systems, Cavendish Laboratory, Department of Physics, University of Cambridge, 19 JJ Thomson Avenue, Cambridge, CB3 0HE, United Kingdom

[‡]Institute of Life Sciences and Department of Chemistry, University of Southampton, Highfield Campus, SO17 1BJ, Southampton, United Kingdom

[†]John van Geest Centre for Brain Repair, University of Cambridge, Forvie Site, Robinson Way, Cambridge, CB2 0PY, United Kingdom

[§]Cambridge Advanced Imaging Centre, Dept. of Physiology, Development and Neuroscience, Anatomy Building, Cambridge University, Downing Street, Cambridge CB2 3DY, UK

KEYWORDS: Surface-enhanced Raman spectroscopy, endocytosis, endosomes, lysosomes, linear discriminant analysis, chemometrics, cells

ABSTRACT

Surface-enhanced Raman spectroscopy (SERS) is an ultra-sensitive vibrational fingerprinting technique widely used in analytical and biosensing applications. For intracellular sensing, typically gold nanoparticles (AuNPs) are employed as transducers to enhance the otherwise weak Raman spectroscopy signals. Thus the signature patterns of the molecular nanoenvironment around intracellular unlabelled AuNPs can be monitored in a reporter-free manner by SERS. The challenge of selectively identifying molecular changes resulting from cellular processes in large and multidimensional data sets and the lack of simple tools for extracting this information has resulted in limited characterization of fundamental cellular processes by SERS. Here, this shortcoming in analysis of SERS data sets is tackled by developing a suitable methodology of reference-based PCA-LDA (principal component analysis-linear discriminant analysis). This method is validated and exemplarily used to extract spectral features characteristic of the endocytic compartment inside cells. The voluntary uptake through vesicular endocytosis is widely used for the internalisation of AuNPs into cells but the characterization of the individual stages of this pathway has not been carried out. Herein, we use reporter-free SERS to identify the stages of endocytosis of AuNPs in cells, visualize them and map the molecular changes *via* the adaptation and advantageous use of chemometric methods in combination with tailored sample preparation. Thus our study demonstrates the capabilities of reporter-free SERS for intracellular analysis and its ability to provide a way of characterizing intracellular composition. The developed analytical approach is generic and enables the application of reporter-free SERS to identify unknown components in different biological matrices and materials.

During the last decade, nanoparticle-based surface-enhanced Raman spectroscopy (SERS) has been extensively employed to study biological systems such as cells and tissues.[1-3] There are primarily two approaches: The SERS reporter approach and the label-free (reporter-free) SERS approach. In the former, a molecule is functionalized as a self-assembled monolayer on the nanoparticle and the SERS detection of its characteristic spectrum serves to visualize the location of the nanoparticle(s) inside the cell or tissue.[1, 2] This SERS reporter approach has been used in a variety of applications including detection of pathologic cells and tissues such as in cancer[4-6] or cancer markers in biofluids such as blood.[7, 8] The reporters can also serve as pH sensors by an appropriate choice of the functionalized molecule with an exchangeable H^+.[9]

On the other hand, reporter-free SERS samples the direct environment in the vicinity of the nanoparticles and makes the spectral features contributed by the multiple molecular components available for the identification and understanding of the molecular changes around them. The nanoparticle probes can be tailored, such as by sparse functionalization, to be delivered inside cells and to specific compartments adding another dimension to their usefulness.[10, 11] Reporter-free SERS, especially involving spatially resolved maps, however, can generate large and complex data sets which require more sophisticated analysis methods to extract significant features.[3] An accompanying complication especially with the reporter-free SERS methodology in cells is that the variation in the state of aggregation can result in a large variation of the intensity and the spatial distribution of the measured spectra[12, 13] making single or average spectra insufficient for complete sample characterization (or classification). Additionally the use of natural (random) aggregation of spherical nanoparticles inside cells makes it difficult to discern any orientational effects of molecules near surfaces in the SERS spectra. These challenges have been addressed by applying various chemometric methods, such

as principal component (PCA)[10, 14-18] and linear discriminant analysis (LDA),[14, 19, 20] least square regression[14, 21, 22] as well as cluster analysis,[17, 23, 24] which mostly aim at the extraction of representative spectral features for the characterization and/or classification of the sample.[7, 14, 17, 25, 26] Furthermore, traditional SERS analysis, including that in the SERS reporter approach, relies on the comparison of spectra from an unknown sample to either: (i) one or more known reference spectral features from a Raman library/literature or (ii) pure samples of expected components. Thus, the requirement for an existing training or reference group or spectra highlights a critical shortcoming in current methods especially for reporter-free SERS because unlike the SERS-reporter approach the molecules being detected are not necessarily known. Moreover, given the complexity of biological matrices and variation therein, obtaining or generating pure samples only containing the desired spectral reference pattern is not trivial. This makes reporter-free SERS in biological samples, although vastly richer in information content, complex and ambitious compared to the conventional use of SERS in (bio)chemical or materials characterization studies.

Here, we propose the development and use of a modified chemometric method to achieve the identification, visual representation and extraction of unknown constituents from reporter-free SERS data sets which are multicomponent by their very nature. The utility of this methodology is then demonstrated for endocytosis, the process of cellular ingestion of extracellular material and their subsequent digestion and degradation. The choice of endocytosis is both natural and ideal. It has been shown that cells can voluntarily internalize spherical gold nanoparticles (AuNPs) from their environment which on internalization can serve as intracellular SERS nanosensors.[2, 3, 10, 11, 27] Once internalized, AuNPs are trafficked along the endo-lysosomal network inside vesicles (also see Figure 1A) with the help of molecular motors and cytoskeletal

structures.[28] In endosomes molecular sorting and recycling takes place. They further fuse with other incoming cargoes while they mature into late endosomes *via* luminal acidification.[29, 30] Thereafter, secondary lysosomes are formed when mature endosomes merge with primary lysosomes that emerge from the Golgi apparatus. Lysosomes contain enzymes (*e.g.* hydrolase) as well as various macromolecules from other intracellular, catabolic processes and membrane turnover.[29, 31] Although further acidification, molecular digestion and degradation takes place, vesicles with indigestible material, such as AuNPs, become residual bodies and are secreted by the cell *via* exocytosis.[31, 32] Thus, nanoparticles enclosed inside these membrane-bound vesicles *witness* the whole maturation process from endosomes to lysosomes and thus are best placed to report the dynamic changes in the intravesicular molecular composition *via* the consequent and inevitable modification of molecules near the surface of AuNPs.[2, 33] Furthermore, these conditions support/favour the formation of intravesicular AuNP aggregates due to vesicle fusion as well as the acidic environment which creates ideal conditions for giving rise to strong SERS enhancements.[3]

Furthermore, while the endo-lysosomal pathway is extremely important for many intracellular functions, there have been relatively few studies using SERS to explore and characterise this pathway.[2, 3] SERS-based investigations within the endocytic pathway have mainly been centred on pH sensing of vesicles,[2, 3, 9, 17, 34-39] always employing reporter molecules such as para-aminothiophenol.[2, 17] Although, the nanoenvironment surrounding the SERS probes has been observed to constantly change, there is lack of information on compartment-specific molecular changes.[2, 17] Thus, despite the importance of this pathway for the intake and exit of SERS nanoparticle probes, the vesicles themselves have not been studied or characterized.[2, 3, 40-42] While Ando *et al.* have studied selective time points during the first minutes to hours of the

cellular intake process, focussing on single-particle tracking in combination with SERS measurements,[40, 42] Kneipp and co-workers have studied the level of SERS enhancement during the first three hours of AuNP intake and the role of adenosine mono- and triphosphate-based acidification in endosomal maturation.[2, 41] To the best of our knowledge, no SERS study has aimed at characterizing of or distinguishing between the molecular content of vesicles, namely endosomes and lysosomes, involved in the different stages of endocytosis.

In this work, we develop a chemometric methodology used to extract features/components from complex SERS data sets. This method is exemplarily applied to cell samples to shed light on the molecular make-up of endosomes and lysosomes employing a reporter-free SERS approach. The experimental methodology and statistical data analysis are used in combination to allow for the generation of a reference sample that can then be employed for a differential analysis of SERS data sets. This method termed reference-based PCA-LDA analysis allows for the identification of unknown (molecular) spectral features within a data set, which in this case corresponds to the endosomes. The method is further successfully applied to generate a color coded distribution of PCA-LDA derived spectral features in SERS maps of cells allowing for the visualization of endosomes and lysosomes within SH-SY5Y human neuroblastoma cells. This enables the detailed hyperspectral characterization of endosomes and lysosomes as well as the determination of the precise vesicular localization of nanoparticles during the uptake process at the same time. As such our study paves the way for the extraction and improved characterization of unknown components and structures using the reporter-free SERS approach inside cells.

RESULTS AND DISCUSSION

We first introduce the methodology for the extraction of the unknown features from a hyperspectral data set and subsequent generation of pseudo-color SERS maps. By adapting the experimental methodology, we created a sample wherein the internalized AuNPs are all in a particular stage of the endo-lysosomal pathway. This creates a 'reference state' used for developing our chemometric methodology termed reference-based PCA-LDA. This is described in the context of the endo-lysosomal pathway and is used to investigate the molecular content of the vesicle types, *i.e.* endosomes and lysosomes.

Experimental design based on the pulse-depletion technique to generate a 'reference state'

In this work, the conventional pulse-chase technique[41, 43] was modified to create a reference state as shown in Figure 1. Briefly, an *incubation pulse* with AuNPs in the cell culture medium (Figure 1A.ii) of 72 h (for details see Materials and Methods) was used to allow for the uptake of a large number of particles in order to allow for them to sample the molecular diversity inside cells and to also allow for the generation of high SERS signals. After the incubation pulse AuNPs are expected to be localized in all types of endocytic vesicles, *i.e.* endosomes (green vesicles) and lysosomes (blue vesicles, schematic in Figure 1B.i). SERS map data from these cells with AuNPs, which are present in both endosomes as well as lysosomes, was acquired and is called the *sample group*. To create a reference state, cells underwent the same incubation pulse but then were washed to remove all extracellular AuNPs and incubated in fresh medium without any AuNPs for 48 h (Figure 1A.iii). This is referred to as the *depletion phase*. This depletion pulse time was optimized (described in next section) and ensures that all of the internalized AuNPs end

up in lysosomes and are completely absent from the endosomes (Figure 1B.ii). SERS data from cells with only lysosomal AuNPs is termed the *reference group*.

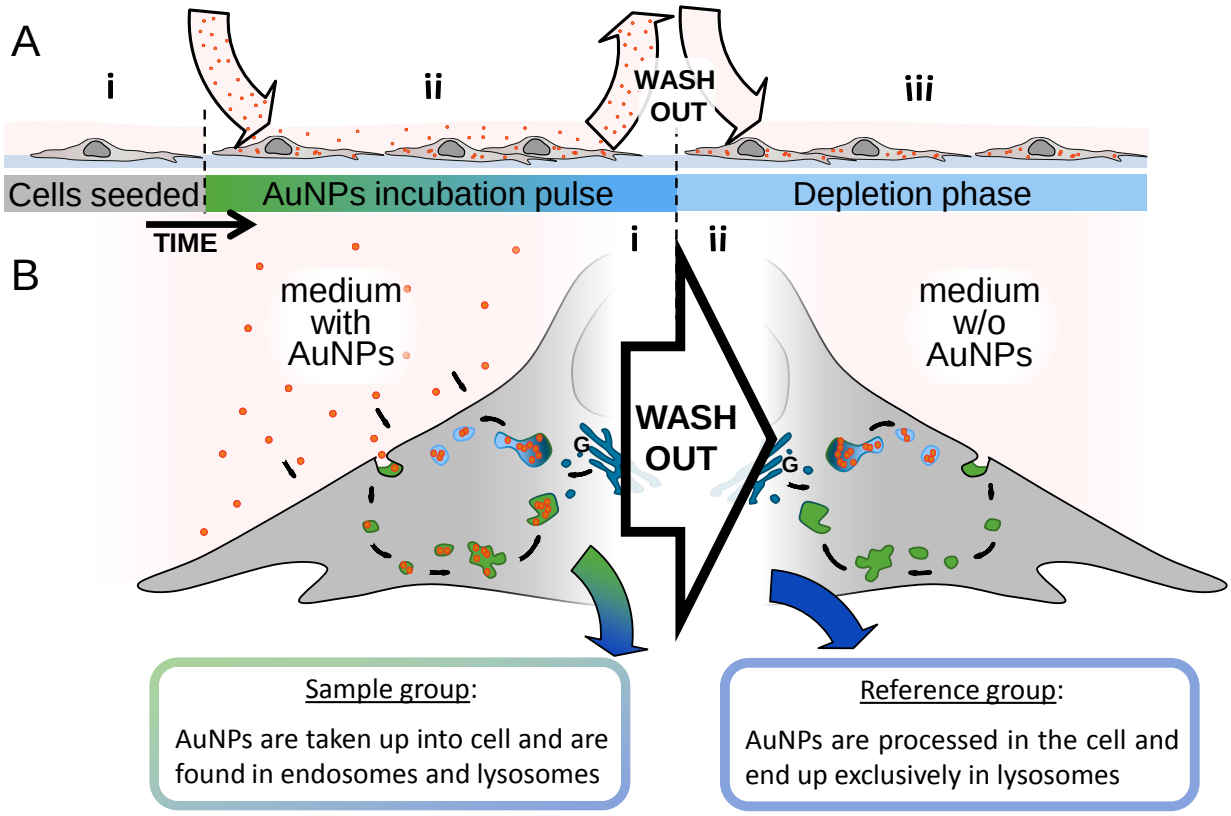

Figure 1: Schematic of experimental design. (A) Full experimental procedure involves AuNPs (red spheres) being added to the cell culture environment after (A.i) cells have sufficiently attached to the culture dish. (A.ii) Following uptake of the particles into the cell *via* endocytosis during the incubation pulse, extracellular particles were washed out. (A.iii) Fresh culture medium without AuNPs was added and the cells were left until incorporated particles were processed into lysosomes (depletion phase). (B.i) During the incubation phase, cells constantly internalize AuNPs, which accumulate inside endosomes (green vesicles) and lysosomes (blue vesicles). Their acquired SERS map data serves as the sample group for analysis. (B.ii) Following the wash-out, vesicular AuNPs are processed along the endo-lysosomal pathway and are eventually found exclusively in lysosomes. SERS maps of fixed cells with only lysosomal AuNPs serve as the reference group for the data analysis. Golgi apparatus (G).

Verification of the pulse-depletion method to create a reference state and to confirm the location of the AuNPs

We verified our pulse-depletion approach in its ability to achieve the required differential localization by using transmission electron (TEM) and fluorescence microscopy. TEM micrographs in Figure 2A-D show representative examples of the intracellular localization of 40 nm AuNPs inside membrane-bound vesicles of the endo-lysosomal system in human neuroblastoma cells (SH-SY5Y cell line). As expected, immediately after the incubation pulse, AuNPs are found in both endosomal (including phagosomes, green arrow) as well as lysosomal vesicles (phagolysosomes and secondary lysosomes, blue arrow) as seen in Figure 2A (also see Supporting Information Figure S1). TEM micrographs were further obtained after a depletion phase of 24 h, 48 h and 72 h as shown in Figure 2B-D to confirm the localization of AuNPs in lysosomes only – the reference state. Although all three TEM micrographs (B-D) showed only marginal differences, it is clear that a depletion time of 48 h was adequate to ensure that all intravesicular AuNPs were processed into lysosomes.

Fluorescence microscopy further confirmed the results obtained by TEM imaging (Figure 2D-E). For cells, imaged directly after the incubation pulse (Figure 2D), clusters of AuNPs (recognizable as black spots) co-localized with the immunofluorescence labelling of lysosomes (red) and endosomes (green). In contrast, after a depletion phase of 48 h, AuNPs only co-localized with the lysosomes (red). Based on the evidence from TEM and fluorescence microscopy experiments, a depletion time of 48 h was chosen for generating the *reference* group data. Metabolic and integrity tests were carried out on the cells throughout the incubation and

depletion phases and showed that the AuNPs had very little effect on the cellular health and viability of the cells (see Supporting Information Figure S2).

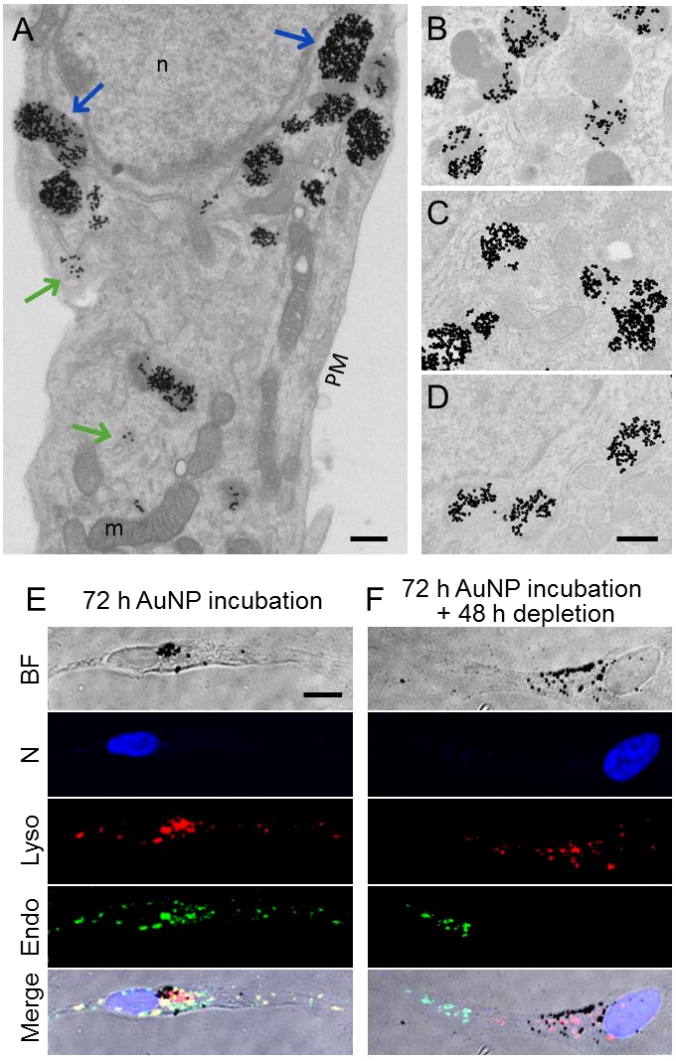

Figure 2: TEM (A-D) and fluorescence images (E-F) of neuroblastoma cells after incubation and depletion pulses. (A) After an AuNP incubation pulse aggregates of different sizes are found in endosomal vesicles (endosomes and phagosomes, green arrow) as well as lysosomal vesicles (phagolysosomes and secondary lysosomes, blue arrows). Following a depletion phase of 24 h (B), 48 h (C) or 72 h (D), AuNPs aggregates of different sizes were found in lysosomes only. (A-D) Scale bar: 500 nm. Additionally, fluorescence microscopy images using stains for the nucleus (N: blue), endosomes

(Endo: green) and lysosomes (Lyso: red) confirmed the localization of AuNPs (E) in endosomes and lysosomes at the end of the incubation pulse and (F) only in lysosomes after 48 h of depletion pulse. (E-F) Scale bar: 10 μm. PM (plasma membrane), m (mitochondrion), n (nucleus).

Analytical approach for the Visualization of two classes in SERS maps: Imaging endosomes and lysosomes in a SERS map of a cell

By using the aforementioned experimental conditions, we thus successfully created two groups for SERS mapping experiments; the *sample* group (n_{sample} = 20) containing SERS probes in both endosomes and lysosomes and the *reference* group ($n_{reference}$ = 14) containing SERS probes in the lysosomes only. The analytical method developed here allows then for the characterization and mapping out of both endosomes and lysosomes within the cells in addition to the extraction of differential spectral features (see also Supporting Information Figure S3). The details of the methodology are described using an exemplar whole cell containing AuNPs in endosomes and lysosomes as shown in the bright-field image in

Figure 3A. A SERS map of the same cell showing integrated intensity in the spectral range (400 - 2000 cm^{-1}) is presented in

Figure 3B. Exemplar SERS spectra from different map positions (indicated by corresponding colored markers in Figure 3B) are shown in Figure 3C. The spectra represent the variation that occurs within endocytic vesicles of a cell. The large amount of spectral data collected in a SERS map and the variation between spectra necessitates the use of chemometric tools to extract the high amount of information in them which goes well beyond single or an average spectrum from a cell.

i) Background exclusion from map scans. In a first step, it is necessary to identify and discard the sample background, areas where the SERS effect is absent as there are no AuNPs present, both inside and outside the cell. For objective discarding of the sample background rather than by subjectively adjusting the look-up table (LUT) in intensity maps or excluding spectra of low intensity, a low-level correlation based method was implemented which considered the main spectral features, identified through principal component analysis (PCA). PCA is an unsupervised multivariate method, increasingly used for spectral characterization of SERS from inside cells and/or intracellular processes.[10, 14-18] PC loadings are commonly used to identify features within the data set which best explain the variance in the data.[44] The spectrum-like PC loadings characterise the main spectral features with the highest significance in the data (*e.g.* peaks in a SERS spectrum)[45] as well as they correlate the corresponding PC score to the original data.

Here background exclusion was objectively carried out using PC scores. Prior to PCA, spectra were baseline-corrected and mean-centred, as described previously.[10, 45] We considered only the first principal component (PC1) and thus only use PC1 score values to discriminate the sample background. All spectra which corresponded to PC1 scores lower than 25% of the maximal value were discarded Figure 4A shows the spatial distribution of the PC1 scores, normalized to [0, 1], within the cell map. All values below 0.25 (in white) correlate well with the intensity based sample background (black) in the original SERS map in

Figure 3B. The aim was to reduce the number of spectra which do not relate to the endosomal and lysosomal vesicles.

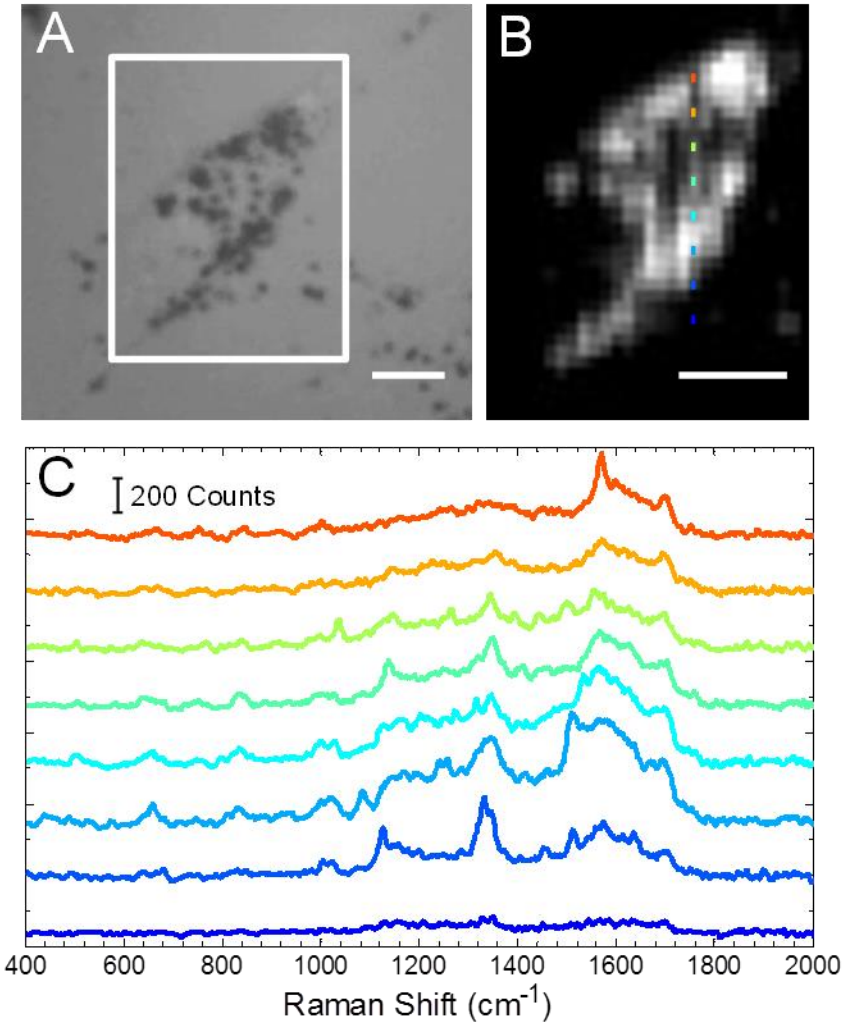

Figure 3: Cellular SERS imaging. A bright-field image (A) within which the box outlines the area scanned for SERS mapping. The corresponding SERS map showing the absolute intensity distribution (integrated over 400-2000 cm^{-1}) is shown in (B). Eight spectra (C) from different positions within the SERS map (indicated by corresponding colored markers in (B)) illustrate the chemical variation sampled by SERS nanoprobes inside endocytic vesicles. Scale bars: 10 μm.

ii) Classification of SERS spectra: Assignment of spectra to endosomes and lysosomes. In a second step, a modified way of applying PCA followed by linear discriminant analysis (LDA), called reference-based PCA-LDA, was used to assign the remaining spectra to either endosomes or lysosomes. LDA allows for the transformation of PC data to achieve maximum segregation based on differences in features. The assignment of the spectra to endosomes or lysosomes was based on their correlation to hyperspectral SERS features of the reference group (cells after pulse-depletion; Figure 1B). Without applying our reference based method a simple color-coded PCA-LD1 scores map is shown in Figure 4. It shows that areas classified as sample background (white areas in Figure 4) do not necessarily correlate to a specific range of LD1 scores (see Supporting Information, Figure S4 for a PC1 vs. LD1 scores plot). LD1 scores are thus inadequate in themselves to visualize and therefore assign corresponding spectra to different types of intracellular vesicles.

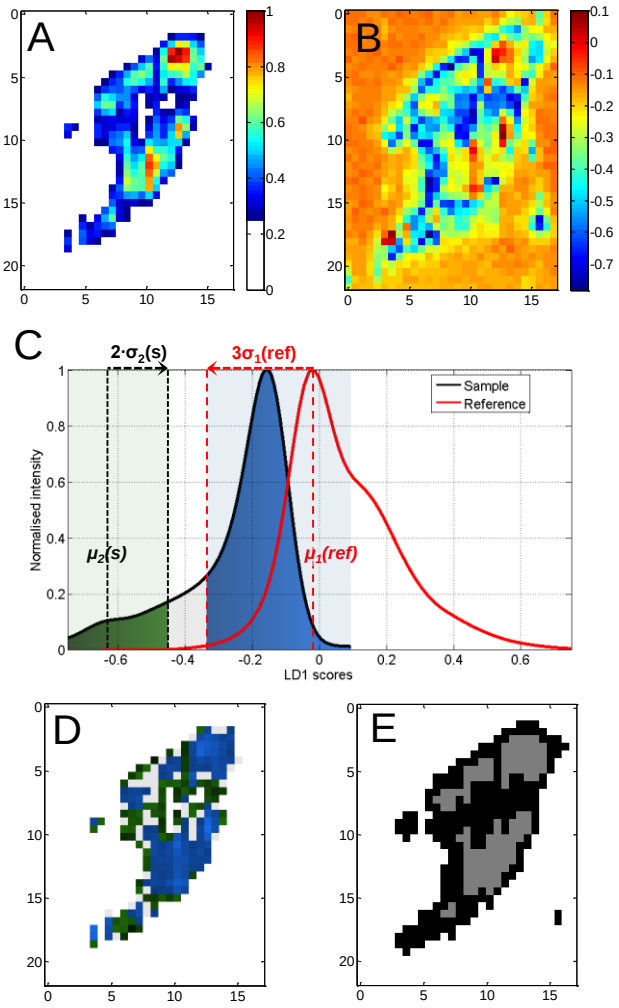

Figure 4: Demonstration with a test sample cell of different analysis steps and comparisons. Pseudo colour PC1 intensity map (A) of the same cell (as in Fig. 3) after PC analysis shows the sample background as white for PC1 scores values smaller 0.25. LD1 scores map (B) of the sample cell prior to endosomes/lysosomes classification. (C) Assignment of components from the LD1 scores intensity distribution to either lysosomes (LD1(s) > -0.35) or endosomes (LD1(s) < -0.45) highlighted in blue and green, respectively. Assignments were made with respect to the modes $\mu_1(ref)$ and $\mu_2(s)$ as well as the standard deviations $\sigma_1(ref)$ and $\sigma_2(s)$ marked as dotted lines. The light grey region between the green and blue regions is a transition region to guarantee an accurate classification. (D) Based on scores for respective class assignments

derived from (C), scores were projected back into a false-color map. This generates a color-coded reference-based PCA-LDA map showing endosomes (green) and lysosomes (blue). (E) A color map was reconstructed after k-means clustering of the test data set for the three groups (white, grey, black) confirming the group segregation facilitated using our color-coded reference-based PCA-LDA method. Pixel size: 600 nm x 600 nm.

It is worth noting here that while the PC1 scores map (Figure 4) expresses the inherent correlation to the principal spectrum of the sample data set, the LD1 scores map (Figure 4) reveals only a correlation with respect to each other. Thus the information, which can be used to distinguish the endosomal and lysosomal spectra, is extractable by realising that similar scores in the LD space indicate similar characteristics (*i.e.* the same peak positions and or intensities). Hence we used the LD1 intensity (histogram of LD1 scores) curves of both the sample and the reference to recognize common features in both respective groups. The scores corresponding to the overlapping region (blue shaded region) of the sample and reference histogram curves thus indicate spectral features common to both groups. Since the lysosomal vesicles are common to both groups the spectra corresponding to these scores can be assigned to them. Based on this understanding, a mathematical strategy for segregation of lysosomes can be derived by using parameters of double Gaussian fits to the individual LD1 intensity curves.

The mathematical description of the scores for lysosomal components $LD1_{lysosomes}(s)$ (blue region, Figure 4) is given by:

$$\mu_1(ref) - 3\sigma_1(ref) < LD1_{lysosomes}(s) \leq \max[LD1(s)],$$

where μ_1 refers to the score position of the major mode of the curve and σ_1 to the standard deviation. *ref* and *s* refer to the reference and the sample group, respectively. Maximal class

assignment is ensured by using the projection of three standard deviations of the major mode of the reference curve. Similar criteria thus could be derived for all cases where the reference curve is positively skewed (see Supporting Information).

Based on the same logic, the non-overlapping region of the sample curve can be assigned to SERS from endosomes as it does not share the scores, and consequently spectral features, with the reference group. The assignment of scores, highlighted in green in Figure 4, was based on the fit parameters of the minor mode of the sample curve and can be written as

$$LD1_{endosomes}(s) < \left(\mu_2(s) - 2\sigma_2(s)\right) \wedge \left(LD1_{lysosomes}(s)\right),$$

where the logical operator (Λ) indicates that both conditions must be fulfilled simultaneously. The data classification (endosomal and lysosomal origin, Figure 4) deliberately leaves a gap in the scores between the two groups. This *transition region* allows for the correct classification by excluding borderline cases. After assigning LD1 scores to the classes and colors, back-projection of the data generates a pseudo-color map clearly outlining the localization of the endosomes (green) and lysosomes (blue) within the cell (Figure 4). Furthermore, it allows for the identification of the localization of the intracellular nanosensors within the endo-lysosomal pathway. This scores distribution was subsequently used for several individual cells (see Materials and Methods) to assign their spectra to the two different classes, endosomes and lysosomes, in order to characterize them and understand spectral differences in the context of endo-lysosomal processes.

In order to verify the use of the mathematical rules derived above for group segregation and its applicability to several cell samples, we used the leave-one-out-cross-validation

algorithm. The method was also verified with negative controls, that is, on cells with lysosomes only and the classification was not only accurate but also demonstrated the advantage over single frequency SERS and simple LD1 score maps (for details see Validation section in Supporting Information and Figure S5). On a single cell basis, we used supervised k-means clustering (k=3) as a verification method of spectral classifications achieved by our reference-based PCA-LDA methodology. Results for the exemplar cell considered above are shown in Figure 4. Our reference-based PCA-LDA map in Figure 4 shows broad agreement with the generated *k*-means clusters (Figure 4E). However, the advantage with our method is that class, and hence spectra, assignments are based on the comparison to the reference state and therefore have a physical meaning whereas k-means itself does not allow for unambiguous assignment of clusters to the specific classes such as endosomes and lysosomes.

Further to validate the generic and broad application of our method, we applied our reference-based PCA-LDA method to a non-biological sample. The sample was created by drying a solution of Rhodamine 6G on a silicon substrate and a hyperspectral image was acquired by Raman spectroscopy. While the components here were known and hence verifiable, the application of the same classification rules used above resulted in improved/accurate visualization of the components (see Supporting Information, Figure S3).

iii) Molecular characterization of the endosomal and lysosomal pathways. Earlier studies have demonstrated great similarities and only small differences of SERS spectra derived from the molecular environment of the endo-lysosomal pathway.[2, 3, 40] In order to achieve the ultimate goal of hyperspectral and molecular characterization of endosomal and lysosomal content, subtle differences in spectra from both groups need identification. For this reason, SERS maps were

acquired from 20 individual cells to facilitate a population statistic. Furthermore, to exclude the effect of spectral intensity variation, due to (typical) inhomogeneous SERS enhancements, on the representative characterization of endosomes and lysosomes, all spectra were mean-centered and PCA was applied to each group. PC1 loadings together with weighting by frequency of occurrences further eliminated any dependence of the analysis on low peak intensities as further described below. The PC1 loadings of endosomes (green) and lysosomes (blue) with their standard deviation (red, see materials and Methods), as shown in Figure 5A, indicate striking similarities between them and only marginal differences. Further analysis was carried out by generating histograms over all peak positions within the spectra of both groups, endosomes and lysosomes, separately (see Materials and Methods). In the bar chart in Figure 5B, the frequency of peak occurrence is shown for endosomal (green, top) as well as lysosomal spectra (blue, bottom). The frequency of occurrence of a peak thus relates directly to its probability.

For a comprehensive characterization of each individual group, information about the peak probability (Figure 5B) was combined with information about peak intensities and ratios (PC1 loadings in Figure 5A). Therefore, for each group the frequency of peak occurrence (normalized to [0 ,1]) was weighted by the PC1 loadings and the difference between the two groups, endosomes and lysosomes, was calculated (Figure 5C) to visualize the spectral changes. Enlargements of sub regions, in particular in the spectral range of 400 – 1050 cm^{-1} are shown in Figure S7 in the supplementary information. Identified changes, which exceed the standard deviation, and assigned molecular processes are highlighted in different colors in Figure 5. These processes are the breakdown of proteins (purple, *p1 – p4*) and lipids (yellow, *y1 – y2*), the rising acidity along the endo-lysosomal pathway (red, *r1 – r4*) and the degradation of DNA/RNA in the

lysosomal system (grey, *g1 – g2*). The spectral changes with respect to each of these processes are discussed in detail below.

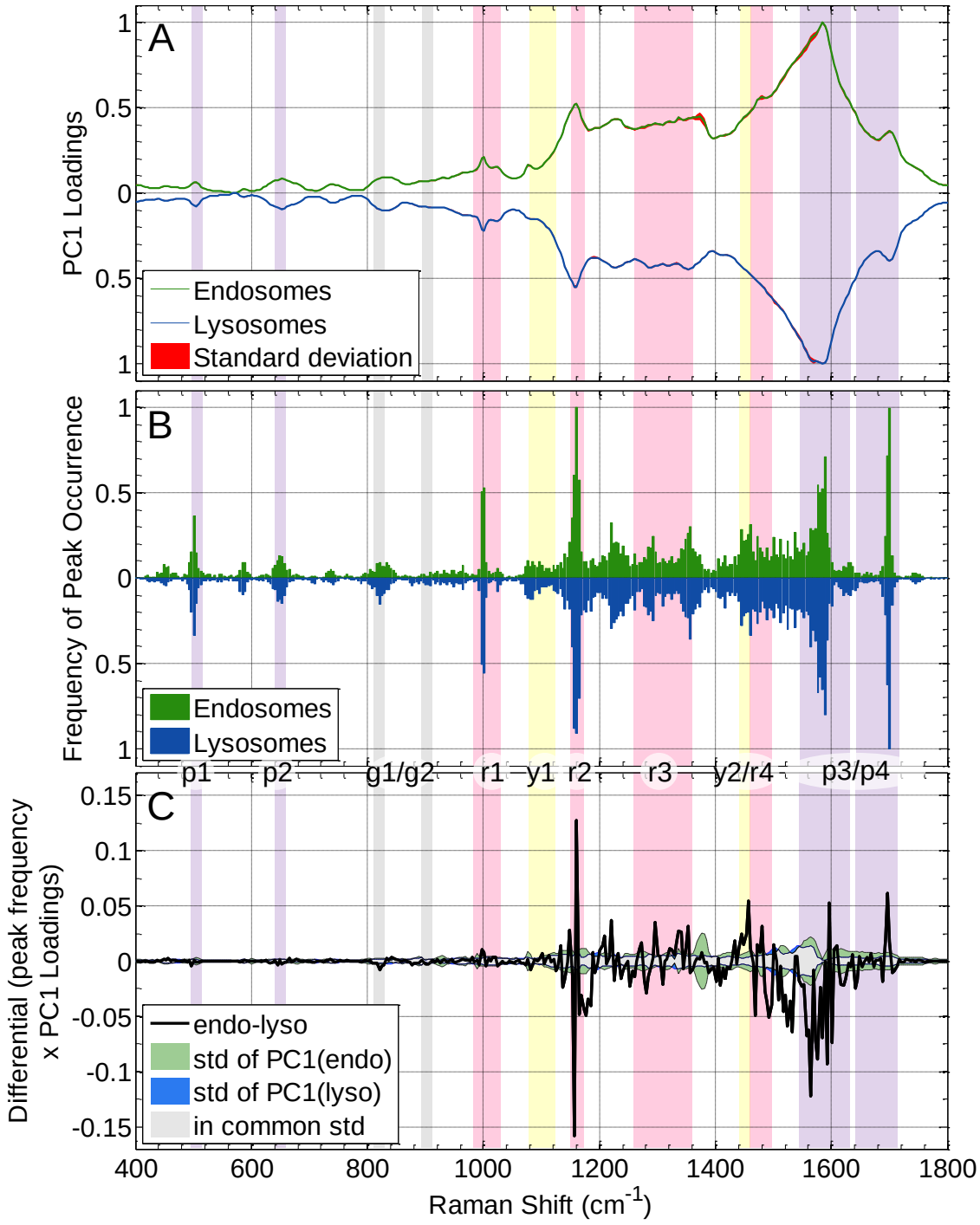

Figure 5: Analysis of spectra specific to the endosomal and lysosomal pathway. (A) Normalized PC1 loadings of all extracted spectra originating from endosomes (green) and lysosomes (blue)

with their standard deviation highlighted in red. (B) The histogram summarizes the (normalized) occurrence probability of SERS peaks from endosomes (green bars) and lysosomes (blue bars). (C) Difference between the PC1 loadings (A) weighted by the frequency of peak occurrence (B) of endosomes and lysosomes. The corresponding standard deviations are shown in green (endosomes), blue (lysosomes) and grey (both groups). Strong minima and maxima suggest major differences between both groups. Highlighted regions refer to molecular processes in the endo-lysosomal system such as the breakdown of proteins (purple, p1-p4) and lipids (yellow, y1-y3), the rising acidity along this pathway (red, r1-r4) and the degradation of DNA/RNA in the lysosomal system (grey, g1 and g2). Marked regions are as following (in cm^{-1}): p1: ~500; p2: 640 – 650, p3: 1550 – 1640; p4: 1625 – 1700; y1: 1080 – 1130; y2: 1440 – 1460; r1: 980 – 1030; r2: ~1160; r3: 1270 – 1370; r4: 1470 – 1500; g1: 808 – 830; g2: 880 – 910.

Breakdown of Proteins and Lipids

The endo-lysosomal pathway is a protein-rich environment which is a major protein degradation pathway within the cell where they are subject to structural changes and denaturation[46]. Bond conformations are related to the structure of the protein and can be observed by SERS. SERS bands related to relevant proteins and peptides as well as fatty acids are highlighted in purple and red in Figure 5, respectively.

S-S stretching vibrations, such as for example in the cysteine-cysteine disulfide bond, result in a strong band at 500 cm^{-1} (purple band *p1* in Figure 5A-B).[47-49] In lysosomes, this band is slightly decreased, which suggests the break-down of polypeptides. In light of this, the increase in the band at 640 – 650 cm^{-1} (bands *p2* in Figure 5), corresponding to the C-S vibrational stretch mode, is related to a better accessibility of the C-S bond in smaller peptides and thus a stronger interaction with the AuNP's surface, compared to unbroken proteins where this bond is hidden

within the protein structure and less accessible for bonding with the surface of AuNPs.[50] Due to the limited access to the protein secondary structure, SERS spectra only rarely show peaks in the amide I region (~1625 – 1690 cm^{-1}),[51] which explains the limited occurrence of peaks from this region in spectra of the endo-lysosomal system. Nevertheless, the weak SERS band at around 1629 – 1637 cm^{-1} can be assigned to the α-helix conformation of the secondary protein structure,[52] which is found to be decreased in lysosomes (see *p3* in Figure 5). Moreover, an increase around 1641 cm^{-1} and 1673 cm^{-1} in lysosomes suggests a related increment of random coil conformation in polypeptides.[53] The modification of intrapeptide hydrogen bonds corresponding to the band at 1629 – 1637 cm^{-1}, which determine and stabilize the secondary structure of proteins, indicates a structural change of proteins and polypeptides, namely their dissociation into polypeptides and fragments of it in the endo-lysosomal system.[46] As a consequence of this degradation, NH_2 groups and N-H bonds are more accessible for binding to the surface of AuNPs and in addition the NH_2 group is protonated to form NH_3^+ in the lysosomal system because of the more acidic pH found within it.[46, 54, 55] This is indicated by a change in the frequency of the SERS peak for the N-H hydrogen bond at around 1700 cm^{-1} in endosomes, with it shifting to 1640 – 1645 cm^{-1} (asymmetric NH_3^+ deformation) in lysosomes. This is shown by the purple bar *p4* in Figure 5A-C[50, 51] and is also supported by an increase in the band at around 1560 – 1600 cm^{-1} in lysosomes, which can be assigned to the asymmetric COO^- stretching vibration.[47]

Alongside protein degradation, the dissociation of lipids also occurs in the endo-lysosomal system. Lipid molecules are broken down into the head group and the tail chain as also suggested by vibrational changes *y1-4* in Figure 5A-B. Generally, lipid bilayers undergo a phase transition (melting), which depends on changes in the environmental conditions such as temperature,

concentration and acidity.[47] In endosomes, the SERS band between 1090 – 1100 cm^{-1} (*y1*) is a superposition of the symmetric PO_2^- vibration stretch of the lipid head group with the C-C stretch of the acyl chain. In lysosomes, this band is decreased and downshifted to 1077 – 1082 cm^{-1} (also *y1*) suggesting an increase in available and accessible C-C bonds of the lipid backbone.[47, 56] Similar behavior has been observed by Carrier and co-workers in the context of temperature induced melting of lipid bilayers and this denaturation study can be compared to the acid-mediated break down of lipids such as it takes place in the endo-lysosomal pathway.[47, 56] At the same time, a shift of the skeletal stretching mode was observed from 1125 – 1130 cm^{-1} in endosomes to 1120 cm^{-1} in lysosomes (also *y1*). This might originate from the sensitivity of the skeletal stretching mode to intrachain disorder and rearrangements as previously observed by Carrie and co-workers.[56] This observed band around 1125 cm^{-1} in endosomes is also in agreement with experimental results of Ando *et al* involving SERS on live cells looking at early endosomal vesicles.[42] The breakdown of lipids affects the structural conformation of the lipid backbone and the decrease of the band around 1440 – 1460 cm^{-1} (*y2*) in lysosomes supports this assertion, as this region is assigned to the scissoring and rocking vibrations of CH_2 and stretching vibration of CH_3.[47, 57]

Changes in SERS in endosomes and lysosomes related to pH

The degradation of proteins as well as lipids is mediated by a decreasing pH throughout the endo-lysosomal pathway. While the extracellular medium and early endosomal vesicles have a pH of around 7.4 – 7.0, the pH decreases down to 6 during endosomal maturation[58] and even 4.5 – 5 in lysosomes to support their digestive enzyme activity. Since amino acids have $–NH_2$ as well as –COOH groups their spectra ought to reflect changes due to this change in pH. However, except for histidine, their pK_a values are outside the upper physiological range of change in the endo-lysosomal system. The imidazole functional group of histidine has a pK_a of 6 with three

additional sites for (pH-related) (de)protonation and therefore shows significant structural changes for a pH decrease from around 7 to 5, which is reflected in the shift of several SERS bands. SERS bands between 1275 to 1300 cm^{-1} are assigned to coupled skeletal CH_2 stretching and bending modes of imidazole as seen in the red band *r3* in Figure 5. Similarly, the =C-H in-plane bending and ring breathing frequency around 1285 – 1300 cm^{-1} assigned to imidazole[59, 60] in endosomes shifts down to 1275 – 1285 cm^{-1} in lysosomes. A strong peak at 1349 – 1357 cm^{-1} in endosomes is assigned to the coupled =N-C and C=N ring stretch in imidazole[60]. This peak overlays with the CH_2 wagging mode found at 1325 cm^{-1} in endosomes and shifted up to 1370 cm^{-1} in lysosomes possibly due to the lower pH.[60] Furthermore, the N-H in plane bending coupled with the C=N skeletal stretch of the imidazole ring[60] shifts higher from 1472 – 1482 cm^{-1} in endosomes to 1485 – 1497 cm^{-1} in the lysosomes as indicated by the differential frequency change in the *r4* band.

Furthermore, modifications of the functional groups of amino acids or the general acidification of the molecular environment can alter backbone vibrations of polypeptide. This is suggested by the marginal shift from 1161 to 1157 cm^{-1} from endosomes to lysosomes (*r2* in Figure 5). This band is assigned to the C-C stretching vibration.[60] Additionally, this shift can also be due to ring N-H deformation coupled to the C=N stretch, which has been observed by Mesu and co-workers and found to be prominent around 1160 – 1164 cm^{-1} for a pH higher than 6 and to disappear for a pH lower than 5.[60] Finally, the *r1* band mainly reflects phosphate peaks in both endosomes and lysosomes. While the frequency of the aromatic breathing mode of phenylalanine is around 1000 cm^{-1} [50, 61] and decreases in lysosomes, an overlap with the phosphate stretching mode at around 980 cm^{-1} [61] can be assumed in endosomes. Furthermore, the effect of a pH decrease might

be responsible for the shift of the PO_2^- peak[61] around 1010 –1020 cm^{-1} in endosomes up to 1025 – 1030 cm^{-1} in lysosomes.

Degradation of DNA/RNA in Lysosomes

Prominent DNA/RNA regions within the SERS spectra are highlighted as *g1* and *g2* (grey bands). In particular, peaks around 808 – 830 cm^{-1} and 880 – 910 cm^{-1} assigned to the O-P-O stretching mode and the ribose phosphate backbone of DNA/RNA, respectively, were found to be more frequent in lysosomes.[62-64] At the same time, peaks at 1533, 1585 and 1592 cm^{-1} can be assigned to the DNA/RNA nucleobase adenine and are pronounced in lysosomes (not indicated in Figure 5). Fujiwara and co-workers have shown the existence of an autophagic pathway, in which DNA and RNA are delivered into lysosomes for their degradation.[65, 66] In this context, the observed SERS regions *g1-2* appear to be indicative of the degradation of DNA/RNA in lysosomes.[65]

CONCLUSION

In this study, we introduced a reference-based PCA-LDA scores differential analysis methodology for the extraction of unknown features/spectra from a hyperspectral data set, subsequent generation of pseudo-color SERS maps and biochemical SERS characterization. To demonstrate its generic applicability, this methodology is exemplarily applied to study endocytosis with reporter-free SERS. Using this method in combination with an experimental AuNPs pulse-depletion approach, we were able to achieve a segregation of spectra from the endosomal and lysosomal pathways within the endocytic uptake system. Results were used to generate pseudo-color maps indicating the distribution of endosomes and lysosomes

corresponding to the uptake of AuNP reporter-free SERS probes. Furthermore, a comparison of molecular and hyperspectral features enabled us to characterize various aspects of the degradation pathway such as the breakdown of proteins and lipids, the increasing acidity along it as well as the degradation of nucleic acids in lysosomes. Our findings of the environment within this important intake route for nanoparticles into cells provide a SERS characterization of the molecular surroundings which they face inside cells. On this basis, our approach combined with advanced sample preparation, for instance using targeted SERS probes, can be used to achieve a further deconvolution of endocytic vesicles towards a holistic molecular characterization of endocytosis. The generic analytical method developed here provides a tool for dealing with complex reporter-free SERS data sets especially from biological matrices and understand biomolecular mechanisms.

MATERIALS AND METHODS

Cell culture. SH-SY5Y cells were cultured in 87% Dulbecco's Modified Eagle's Medium (GIBCO), 10% heat inactivated fetal bovine serum (PAA), 2% B-27® (GIBCO) and 1% Antitibiotic-Antimycoticum (GIBCO) at 37°C in a humidified atmosphere. For experiments, cellular differentiation into a non-dividing phenotype was achieved adding 10 nM staurosporine (Sigma) to the medium. After at least 3 days, cells were re-seeded on sterile, poly-L-lysine (Sigma) glass coverslips (13 mm) at a density of ~$3.8 \cdot 10^4$ cells/mm^2 and left for 24 h before experimental use. For SERS experiments citrate-capped, spherical gold nanoparticles (BBintenational, UK) of 40 nm diameter in suspension with culture medium (final particle concentration of ~$1.1 \cdot 10^{-10}$ M) were added for 72 h to the cells. Thereafter, cells of the sample group were washed and fixed with 4% formaldehyde (for 10 min). Cells for a second sample group (reference state) were washed, suspended with fresh, particle-free culture medium and left for another 48 h in the incubator before final fixation.

Cell viability, staining and imaging. Trypan blue/dye exclusion method: To assess cell membrane integrity as an indicator of cell viability, differentiated SH-SY5Y cells were seeded at ~10^4 cell per well in a 96-well plate (flat bottom, 0.3165 mm^2) for different particle incubation and depletion conditions as described above. Immediately after treatment, cells were incubated with 100 µl accutase (Sigma) per well for 20 min in order to detach the cells. Once detached, cells were re-suspended, centrifuged with 200 µl of culture medium, the supernatant was then removed and 10 µl of the final cell solution was added to 10 µl of 0.4% trypan blue solution. 10 µl of the mixture were loaded to the Countess® Automated Cell Counter slides. Cells were allowed to sit for 2 min, and the % of surviving cells was read using the Countess® Automated Cell Counter. This was repeated six times for each sample.

Resazurin fluorometric method: To assess cell oxidation/reduction as an indicator of cell metabolism, differentiated SH-SY5Y cells were seeded at ~10^4 cells per well in a 96-well plate. Resazurin cell viability assay was performed as described by the manufacturer (Biotum 30025-1). In short, 15 µl/well resazurin was added to the culture medium and incubated for 3 h. Colorimetric absorbance was measured at 570 nm and 600 nm and the results obtained using $OD_{570} - OD_{600}$.

Endosome and lysosome staining: To assess the subcellular localization of AuNPs in the endo-lysosomal pathway, cells were transfected with CellLight® Endosomes-GFP and CellLight® Lysosomes-RFP, BacMam 2.0, at 120 h after AuNP incubation. Co-localization of AuNPs and endosomes/lysosomes were conducted using confocal analysis.

Transmission electron microscopy (TEM): Following treatment of cells with the AuNPs as indicated, cells were washed three times in 0.9% saline and fixed in 3% glutaraldehyde/1% formaldehyde in 0.05 M sodium cacodylate buffer at pH 7.2 for 2 h at 4°C. Fixed cells were scraped and washed another three times in 0.05 M sodium cacodylate buffer. Samples were post-fixed for 1 h at room temperature in 1% osmium tetroxide containing 1.5% potassium ferricyanide in 0.05 M sodium cacodylate buffer pH 7.4. After rinsing 3 times in deionized water, cells were dehydrated by multiple exchanges in progressively higher ethanol concentrations up to 100 %, followed by two exchanges in dry 100% acetonitrile. Afterwards, samples were left in 50 % acetonitrile/50% Quetol epoxy resin overnight followed by four daily changes of resin (8.75 g Quetol 651 (Agar), 13.75 g Nonenyl Succinic Anhydride (NSA) hardener, 2.5 g Methyl-5-Norbornene-2,3-Dicarboxylic Anhydride (MNA) hardener and 0.62 g Benzyldimethylamine (BDMA) catalyst). Samples were then cured at 60°C for 48 h and thin

sections (80 - 90 nm) were cut using a Leica Ultracut UCT ultramicrotome and collected on bare 300 mesh copper grids. Sections were post-stained using lead citrate and uranyl acetate for 3 min each. Samples were viewed using a Tecnai G2 electron microscope run at 120 keV.

Raman experiments. All SERS experiments were performed using a Renishaw® inVia Raman microscope with a 633 nm laser in streamline mode for map scans (pixel size: 600 nm x 600 nm). A Leica 100x (NA=0.85) objective was used. Measurements were carried out using a collection time of 15-20 s per line of spectra over a spectral range from 400 to 2200 cm^{-1}. The excitation intensity was ~$2 \cdot 10^4$ W/cm^2. Wire 3.4 software was used for data acquisition and initial processing.

Data analysis. Exported raw spectra from map scans were background subtracted using MATLAB 2010b as done previously [10] following mean-centring and vector-normalisation prior to PCA and PCA-LDA analysis. PCA-LDA analysis was carried out using the IRootLab toolbox (https://code.google.com/p/irootlab/) for vibrational spectroscopy.[45, 67] For construction of pseudo-colour maps, PCA and PCA-LDA scores were used as back-projected input information. K-means was performed with MATLAB 2010b for three clusters.

The method of analysis as described in the results and discussion section was carried out for several cell samples ($n = 20$), which were incubated with AuNPs for 72 h (incubation pulse) followed by 48 h of an AuNPs depletion phase. Cells for the sample and reference groups were derived from four independent, experimental repeats. The reference group was formed of 150 SERS spectra each from 14 individual cells with AuNPs localized in lysosomal vesicles only, resulting in a reference pool of 2100 SERS spectra. Spectra from the sample as well as the reference group were baseline-corrected, mean-centred and vector-normalized prior to grouped PCA-LDA processing. Extracted raw spectra from inside the endosomes and lysosomes were

grouped separately; all spectra were baseline-corrected and spectra with a maximal intensity lower than 100 counts (a. u.) were discarded. In this way, characteristic spectra for endosomes and lysosomes ($n_{endosomes} = 1817$, $n_{lysosomes} = 3503$) were obtained for further analysis. PC1 loadings for both groups were generated by applying PCA (see Figure 5A) .The variation within each group was evaluated by comparing subsets of the group data. For each group, 1000 spectra were randomly chosen from the whole data set and PCA was applied. The standard deviation of six repeats is shown as red shaded area. Further analysis was carried out by only taking the peak positions (MATLAB built-in function findpeaks with a minimum peak heights and distance of 15) within the smoothed (moving average filter, span of 21 data points) spectra (see Figure 5B). This was necessary since SERS peaks show quite some variation in their intensities within each group. Histograms with a bin size of 4 cm^{-1} were generated for both groups (endosomes and lysosomes) separately.

ASSOCIATED CONTENT

Supporting Information. Further details on methodology development, validation, TEM images, cell viability data, reference-based PCA-LDA analysis of a non-biological sample and spectral assignments are available as supporting information. This material is available free of charge *via* the Internet at http://pubs.acs.org.

AUTHOR INFORMATION

Corresponding Author

Email: s.mahajan@soton.ac.uk

Author Contributions

AH, RAB and SM conceptualized the project. AH carried out the experiments with help from WLK on the fluorescent and cell based assays. TEM sample preparation and imaging was carried out by KHM and JNS. SM supervised the overall project. The first draft was written by AH and SM and all others contributed thereafter. All authors went through the final version and have given approval of the manuscript.

Funding Sources

Support from the Institute of Life Sciences at the University of Southampton and ERC grant NanoChemBioVision 638258 is gratefully acknowledged. R.A.B. is supported by an National Institute for Health Research (NIHR) award of a Biomedical Research Center to the University of Cambridge and Addenbrooke's Hospital (RG52192). Salary support for A.H. was provided by the NIHR Biomedical Research Grant. We acknowledge funding from the Biomedical Research Unit Cambridge.

ACKNOWLEDGMENT

The useful discussions with Dr Judith M. Fonville and Felix Benz are gratefully acknowledged. We are also highly grateful to Prof. Jeremy J. Baumberg for access to facilities and the Renishaw Raman microscope.

ABBREVIATIONS

AuNP, gold nanoparticle; LDA, linear discriminant analysis; PCA, principal component analysis, R6G, Rhodamine 6G: SERS, surface-enhanced Raman spectroscopy, TEM, transmission electron microscopy.

REFERENCES

1. Schlücker, S. Surface-Enhanced Raman Spectroscopy: Concepts and Chemical Applications. *Angew Chem Int Ed* 2014, 53, 4756-4795.
2. Drescher, D.; Kneipp, J. Nanomaterials in Complex Biological Systems: Insights from Raman Spectroscopy. *Chem Soc Rev* 2012, 41, 5780-5799.
3. Kneipp, J.; Drescher, D. Sers in Cells: From Concepts to Practical Applications. In *Frontiers of Surface-Enhanced Raman Scattering*, John Wiley & Sons, Ltd: 2014; pp 285-308.
4. Mert, S.; Çulha, M. Surface-Enhanced Raman Scattering-Based Detection of Cancerous Renal Cells. *Appl Spectrosc* 2014, 68, 617-624.
5. Li, Z.; Li, C.; Lin, D.; Huang, Z.; Pan, J.; Chen, G.; Lin, J.; Liu, N.; Yu, Y.; Feng, S.*, et al.* Surface-Enhanced Raman Spectroscopy for Differentiation between Benign and Malignant Thyroid Tissues. *Laser Phys Lett* 2014, 11, 045602.
6. Gajjar, K.; Heppenstall, L. D.; Pang, W.; Ashton, K. M.; Trevisan, J.; Patel, I. I.; Llabjani, V.; Stringfellow, H. F.; Martin-Hirsch, P. L.; Dawson, T.*, et al.* Diagnostic Segregation of Human Brain Tumours Using Fourier-Transform Infrared and/or Raman Spectroscopy Coupled with Discriminant Analysis. *Anal Methods* 2013, 5, 89-102.
7. Wang, J.; Zeng, Y. Y.; Lin, J. Q.; Lin, L.; Wang, X. C.; Chen, G. N.; Huang, Z. F.; Li, B. H.; Zeng, H. S.; Chen, R. Sers Spectroscopy and Multivariate Analysis of Globulin in Human Blood. *Laser Phys* 2014, 24, 065602.
8. Guo, L.; Zhang, Y.; Lü, J.-y.; Gao, W.-b.; Wu, S.-f.; Wang, R.-y. Multivariate Statistical Analysis of Serum from Breast Cancer Patients Using Surface Enhanced Raman Spectrum. *Spectrosc Spect Anal* 2013, 33, 1553-1556.
9. Kneipp, J.; Kneipp, H.; Wittig, B.; Kneipp, K. Following the Dynamics of Ph in Endosomes of Live Cells with Sers Nanosensors. *J Phys Chem C* 2010, 114, 7421-7426.
10. Huefner, A.; Kuan, W.-L.; Barker, R. A.; Mahajan, S. Intracellular Sers Nanoprobes for Distinction of Different Neuronal Cell Types. *Nano Lett* 2013, 13, 2463-2470.
11. Huefner, A.; Septiadi, D.; Wilts, B. D.; Patel, I. I.; Kuan, W.-L.; Fragniere, A.; Barker, R. A.; Mahajan, S. Gold Nanoparticles Explore Cells: Cellular Uptake and Their Use as Intracellular Probes. *Methods* 2014, 68, 354-363.
12. Otto, A.; Mrozek, I.; Grabhorn, H.; Akemann, W. Surface-Enhanced Raman Scattering. *J Phys-Condens Mat* 1992, 4, 1143.
13. Joseph, V.; Matschulat, A.; Polte, J.; Rolf, S.; Emmerling, F.; Kneipp, J. Sers Enhancement of Gold Nanospheres of Defined Size. *J Raman Spectrosc* 2011, 42, 1736-1742.
14. Notingher, I.; Jell, G.; Notingher, P. L.; Bisson, I.; Tsigkou, O.; Polak, J. M.; Stevens, M. M.; Hench, L. L. Multivariate Analysis of Raman Spectra for *In Vitro* Non-Invasive Studies of Living Cells. *J Mol Struct* 2005, 744-47, 179-185.
15. Ong, Y. H.; Lim, M.; Liu, Q. Comparison of Principal Component Analysis and Biochemical Component Analysis in Raman Spectroscopy for the Discrimination of Apoptosis and Necrosis in K562 Leukemia Cells: Errata. *Opt Express* 2012, 20, 25041-25043.
16. Pascut, F. C.; Goh, H. T.; Welch, N.; Buttery, L. D.; Denning, C.; Notingher, I. Noninvasive Detection and Imaging of Molecular Markers in Live Cardiomyocytes Derived from Human Embryonic Stem Cells. *Biophys J* 2011, 100, 251-259.
17. Matschulat, A.; Drescher, D.; Kneipp, J. Surface-Enhanced Raman Scattering Hybrid Nanoprobe Multiplexing and Imaging in Biological Systems. *ACS nano* 2010, 4, 3259-3269.

18. Lin, J.; Chen, R.; Feng, S.; Pan, J.; Li, B.; Chen, G.; Lin, S.; Li, C.; Sun, L.-q.; Huang, Z., *et al.* Surface-Enhanced Raman Scattering Spectroscopy for Potential Noninvasive Nasopharyngeal Cancer Detection. *J Raman Spectrosc* 2012, 43, 497-502.
19. Hutchings, J.; Kendall, C.; Shepherd, N.; Barr, H.; Stone, N. Evaluation of Linear Discriminant Analysis for Automated Raman Histological Mapping of Esophageal High-Grade Dysplasia. *J Biomed Opt* 2010, 15, 066015-066015-10.
20. Larraona-Puy, M.; Ghita, A.; Zoladek, A.; Perkins, W.; Varma, S.; Leach, I. H.; Koloydenko, A. A.; Williams, H.; Notingher, I. Development of Raman Microspectroscopy for Automated Detection and Imaging of Basal Cell Carcinoma. *J Biomed Opt* 2009, 14, 054031.
21. Muratore, M. Raman Spectroscopy and Partial Least Squares Analysis in Discrimination of Peripheral Cells Affected by Huntington's Disease. *Anal Chim Acta* 2013, 793, 1-10.
22. Li, X.; Yang, T.; Li, S. Discrimination of Serum Raman Spectroscopy between Normal and Colorectal Cancer Using Selected Parameters and Regression-Discriminant Analysis. *Appl Opt* 2012, 51, 5038-5043.
23. Downes, A.; Elfick, A. Raman Spectroscopy and Related Techniques in Biomedicine. *Sensors* 2010, 10, 1871-1889.
24. Krafft, C.; Dietzek, B.; Popp, J. Raman and Carsmicrospectroscopy of Cells and Tissues. *Analyst* 2009, 134, 1046-1057.
25. Cooper, J. B. Chemometric Analysis of Raman Spectroscopic Data for Process Control Applications. *Chemometr Intell Lab* 1999, 46, 231-247.
26. Sattlecker, M.; Bessant, C.; Smith, J.; Stone, N. Investigation of Support Vector Machines and Raman Spectroscopy for Lymph Node Diagnostics. *Analyst* 2010, 135, 895-901.
27. Kang, B.; Austin, L. A.; El-Sayed, M. A. Observing Real-Time Molecular Event Dynamics of Apoptosis in Living Cancer Cells Using Nuclear-Targeted Plasmonically Enhanced Raman Nanoprobes. *ACS nano* 2014, 8, 4883-4892.
28. Chou, L. Y. T.; Ming, K.; Chan, W. C. W. Strategies for the Intracellular Delivery of Nanoparticles. *Chem Soc Rev* 2011, 40, 233-245.
29. Huotari, J.; Helenius, A. Endosome Maturation. *EMBO J* 2011, 30, 3481-3500.
30. Hillaireau, H.; Couvreur, P. Nanocarriers' Entry into the Cell: Relevance to Drug Delivery. *Cell Mol Life Sci* 2009, 66, 2873-96.
31. Desnick, R. J.; Schuchman, E. H. Enzyme Replacement and Enhancement Therapies: Lessons from Lysosomal Disorders. *Nat Rev Genet* 2002, 3, 954-66.
32. Chithrani, B. D.; Chan, W. C. W. Elucidating the Mechanism of Cellular Uptake and Removal of Protein-Coated Gold Nanoparticles of Different Sizes and Shapes. *Nano Lett* 2007, 7, 1542-1550.
33. Pino, P. d.; Pelaz, B.; Zhang, Q.; Maffre, P.; Nienhaus, G. U.; Parak, W. J. Protein Corona Formation around Nanoparticles - from the Past to the Future. *Mater Horiz* 2014, 1, 301-313.
34. Bálint, Š.; Rao, S.; Marro, M.; Miškovský, P.; Petrov, D. Monitoring of Local Ph in Photodynamic Therapy-Treated Live Cancer Cells Using Surface-Enhanced Raman Scattering Probes. *J Raman Spectrosc* 2011, 42, 1215-1221.
35. Bishnoi, S. W.; Rozell, C. J.; Levin, C. S.; Gheith, M. K.; Johnson, B. R.; Johnson, D. H.; Halas, N. J. All-Optical Nanoscale Ph Meter. *Nano Lett* 2006, 6, 1687-1692.
36. Drescher, D.; Buchner, T.; McNaughton, D.; Kneipp, J. Sers Reveals the Specific Interaction of Silver and Gold Nanoparticles with Hemoglobin and Red Blood Cell Components. *Phy Chem Chem Phys* 2013, 15, 5364-5373.

37. Drescher, D.; Guttmann, P.; Buchner, T.; Werner, S.; Laube, G.; Hornemann, A.; Tarek, B.; Schneider, G.; Kneipp, J. Specific Biomolecule Corona Is Associated with Ring-Shaped Organization of Silver Nanoparticles in Cells. *Nanoscale* 2013.
38. Kneipp, J. Nanosensors Based on Sers for Applications in Living Cells. In *Surface-Enhanced Raman Scattering*, Kneipp, K.; Moskovits, M.; Kneipp, H., Eds. Springer Berlin / Heidelberg: 2006; Vol. 103, pp 335-349.
39. Kneipp, J.; Kneipp, H.; Wittig, B.; Kneipp, K. One- and Two-Photon Excited Optical Ph Probing for Cells Using Surface-Enhanced Raman and Hyper-Raman Nanosensors. *Nano Lett* 2007, 7, 2819-2823.
40. Ando, J.; Fujita, K.; Smith, N. I.; Kawata, S. Dynamic Sers Imaging of Cellular Transport Pathways with Endocytosed Gold Nanoparticles. *Nano Lett* 2011, 11, 5344-5348.
41. Kneipp, J.; Kneipp, H.; McLaughlin, M.; Brown, D.; Kneipp, K. *In Vivo* Molecular Probing of Cellular Compartments with Gold Nanoparticles and Nanoaggregates. *Nano Lett* 2006, 6, 2225-2231.
42. Ando, J.; Yano, T.-a.; Fujita, K.; Kawata, S. Metal Nanoparticles for Nano-Imaging and Nano-Analysis. *Phy Chem Chem Phys* 2013, 15, 13713-13722.
43. Alberts, B. *Molecular Biology of the Cell*. 5th ed.; Garland Science: 2008; p 1268.
44. Abdi, H.; Williams, L. J. Principal Component Analysis. *WIRES Comp Stat* 2010, 2, 433-459.
45. Martin, F. L.; Kelly, J. G.; Llabjani, V.; Martin-Hirsch, P. L.; Patel, I. I.; Trevisan, J.; Fullwood, N. J.; Walsh, M. J. Distinguishing Cell Types or Populations Based on the Computational Analysis of Their Infrared Spectra. *Nat Protocols* 2010, 5, 1748-1760.
46. Alberts, B. *Essential Cell Biology*. 3rd ed.; Garland Science: New York, 2010; p xx, 708 p. (various pagings).
47. Socrates, G.; Socrates, G. I. c. g. f. *Infrared and Raman Characteristic Group Frequencies : Tables and Charts*. 3rd ed.; Wiley: Chichester, 2001; p xv, 347 p.
48. Edsall, J. T.; Otvos, J. W.; Rich, A. Raman Spectra of Amino Acids and Related Compounds. Vii. Glycylglycine, Cysteine, Cystine and Other Amino Acids. *J Am Chem Soc* 1950, 72, 474-477.
49. Tu, A. T. Use of Raman Spectroscopy in Biological Compounds. *J Chin Chem Soc* 2003, 50, 1-10.
50. Podstawka, E.; Ozaki, Y.; Proniewicz, L. M. Part Iii: Surface-Enhanced Raman Scattering of Amino Acids and Their Homodipeptide Monolayers Deposited onto Colloidal Gold Surface. *Appl Spectrosc* 2005, 59, 1516-1526.
51. Kurouski, D.; Postiglione, T.; Deckert-Gaudig, T.; Deckert, V.; Lednev, I. K. Amide I Vibrational Mode Suppression in Surface (Sers) and Tip (Ters) Enhanced Raman Spectra of Protein Specimens. *Analyst* 2013, 138, 1665-1673.
52. Maiti, N. C.; Apetri, M. M.; Zagorski, M. G.; Carey, P. R.; Anderson, V. E. Raman Spectroscopic Characterization of Secondary Structure in Natively Unfolded Proteins: A-Synuclein. *J Am Chem Soc* 2004, 126, 2399-2408.
53. Kurouski, D.; Deckert-Gaudig, T.; Deckert, V.; Lednev, I. K. Structure and Composition of Insulin Fibril Surfaces Probed by Ters. *J Am Chem Soc* 2012, 134, 13323-13329.
54. Mihailescu, G. H.; Olenic, L.; Pruneanu, S.; Bratu, I.; Kacso, I. The Effect of Ph on Amino Acids Binding to Gold Nanoparticles. *J Optoelectron Adv M* 2007, 9, 4.
55. Barth, A.; Zscherp, C. What Vibrations Tell Us About Proteins. *Q Rev Biophys* 2002, 35, 369-430.

56. Carrier, D.; Pézolet, M. Raman Spectroscopic Study of the Interaction of Poly-L-Lysine with Dipalmitoylphosphatidylglycerol Bilayers. *Biophys J* 1984, 46, 497-506.
57. Huang, Z.; McWilliams, A.; Lui, H.; McLean, D. I.; Lam, S.; Zeng, H. Near-Infrared Raman Spectroscopy for Optical Diagnosis of Lung Cancer. *Int J Cancer* 2003, 107, 1047-1052.
58. Celis, J. E. *Cell Biology : A Laboratory Handbook*. 3rd ed ed.; Elsevier Academic Press: Amsterdam, Oxford, 2005; p 4 v.
59. Stewart, S.; Fredericks, P. M. Surface-Enhanced Raman Spectroscopy of Amino Acids Adsorbed on an Electrochemically Prepared Silver Surface. *Spectrochim Acta A* 1999, 55, 1641-1660.
60. Mesu, J. G.; Visser, T.; Soulimani, F.; Weckhuysen, B. M. Infrared and Raman Spectroscopic Study of Ph-Induced Structural Changes of L-Histidine in Aqueous Environment. *Vib Spectrosc* 2005, 39, 114-125.
61. Xie, Y.; Jiang, Y.; Ben-Amotz, D. Detection of Amino Acid and Peptide Phosphate Protonation Using Raman Spectroscopy. *Anal Biochem* 2005, 343, 223-230.
62. Verrier, S.; Notingher, I.; Polak, J. M.; Hench, L. L. *In Situ* Monitoring of Cell Death Using Raman Microspectroscopy. *Biopolymers* 2004, 74, 157-62.
63. Boyd, A.; McManus, L.; Burke, G.; Meenan, B. Raman Spectroscopy of Primary Bovine Aortic Endothelial Cells: A Comparison of Single Cell and Cell Cluster Analysis. *J Mater Sci-Mater M* 2011, 22, 1923-1930.
64. Rao, S.; Raj, S.; Cossins, B.; Marro, M.; Guallar, V.; Petrov, D. Direct Observation of Single DNA Structural Alterations at Low Forces with Surface-Enhanced Raman Scattering. *Biophys J* 2013, 104, 156-162.
65. Fujiwara, Y.; Kikuchi, H.; Aizawa, S.; Furuta, A.; Hatanaka, Y.; Konya, C.; Uchida, K.; Wada, K.; Kabuta, T. Direct Uptake and Degradation of DNA by Lysosomes. *Autophagy* 2013, 9, 1167-71.
66. Fujiwara, Y.; Furuta, A.; Kikuchi, H.; Aizawa, S.; Hatanaka, Y.; Konya, C.; Uchida, K.; Yoshimura, A.; Tamai, Y.; Wada, K.*, et al.* Discovery of a Novel Type of Autophagy Targeting Rna. *Autophagy* 2013, 9, 403-9.
67. Trevisan, J.; Angelov, P. P.; Scott, A. D.; Carmichael, P. L.; Martin, F. L. Irootlab: A Free and Open-Source Matlab Toolbox for Vibrational Biospectroscopy Data Analysis. *Bioinformatics* 2013, 29, 1095-1097.